



 Cite this: *RSC Adv.*, 2024, 14, 24970

Catalytic hydrolysis of methyl mercaptan and methyl thioether on hydroxyl-modified ZrO₂: a density functional theory study†

 Guihua Zhang^a and Xin Song ^{*bc}

The purification and removal of organic sulfur from natural gas is conducive to increasing the added value of natural gas and reducing environmental pollution. In this study, the adsorption properties of methyl mercaptan (CH₃SH), dimethyl sulfide (C₂H₆S) and H₂O on the surface of hydroxyl-modified ZrO₂ were investigated using density functional theory (DFT) calculations. Additionally, a reaction mechanism was proposed for hydroxyl-modified ZrO₂ catalyzing the hydrolysis of CH₃SH and C₂H₆S. The chemisorption of H₂O molecules on the catalyst surface is attributed to H–O and H–Zr bonds. The chemisorption of CH₃SH and C₂H₆S on the catalyst surface is attributed to Zr–S bonds. Competitive adsorption between the three gases exists only between CH₃SH and C₂H₆S. It reveals the water-resistant properties of hydroxyl-modified ZrO₂ in desulfurization. The adsorption energies of the three gas molecules on the hydroxyl-modified ZrO₂ surface are in the order of CH₃SH – (Zr) > C₂H₆S – (Zr) > H₂O – (OH). The natural hydrolysis of CH₃SH and C₂H₆S is a heat-absorbing process that cannot occur spontaneously. The rate-determining step for CH₃SH catalytic hydrolysis is the formation of CH₃O. The fracture of CH₃SHO is the rate-determining step for C₂H₆S catalytic hydrolysis. The depletion of the surface hydroxyl groups can be replenished by the dissociation of H₂O molecules. Hydroxyl-modified ZrO₂ facilitated the hydrolysis process of CH₃SH to a greater extent than that of C₂H₆S. This study provides theoretical guidance for industrial applications and the design of hydroxyl-containing hydrolysis catalysts.

 Received 23rd May 2024
 Accepted 29th July 2024

DOI: 10.1039/d4ra03801k

rsc.li/rsc-advances

1. Introduction

In light of the imperative to sustainably develop the global climate and environment, the energy structure is undergoing continual optimization, with natural gas assuming an increasingly pivotal role in the global primary energy mix. Sulfides such as hydrogen sulfide (H₂S), carbonyl sulfide (COS), methyl mercaptan (CH₃SH) and dimethyl sulfide (C₂H₆S) are common harmful impurities in natural gas, which not only reduce the value of natural gas utilization but also cause corrosion of equipment and environmental pollution.^{1,2} Therefore, the purification of sulfur-containing impurities in natural gas is conducive to environmental protection and effective utilization of natural gas. The purification technologies for H₂S and COS are relatively mature, so the key to natural gas desulfurization is the purification of CH₃SH and C₂H₆S.³

The removal of CH₃SH and C₂H₆S from natural gas is more effectively and stably accomplished using dry methods such as adsorption, catalytic oxidation, catalytic decomposition, and catalytic hydrolysis.^{4–7} Among these methods, the catalytic hydrolysis method has been receiving increasing attention due to its low secondary pollution and high value of by-products. Zhang *et al.* investigated the role of H₂O molecules on CH₃SH removal over Cu/C-PAN catalyst.⁶ It was demonstrated that water promotes the adsorption of CH₃SH at low temperatures and its hydrolysis at high temperatures. While H₂S is the primary hydrolysis product, the reaction temperature and active components influence the type and quantity of the final product. This can diminish the desulfurization stability of the catalyst. Metal oxides, such as ZrO₂, are frequently employed in the purification of gaseous pollutants, exhibiting high reaction stability and resistance to sulfur poisoning.^{8–10} This property is conducive to the stability of the catalytic hydrolysis process of organic sulfur and the prolongation of catalyst service life.¹¹ Therefore, ZrO₂ can be considered a potential hydrolysis catalyst for the purification of organic sulfur. Furthermore, hydroxyl groups play a pivotal role in the hydrolysis of organic sulfur. These groups are primarily derived from the dissociation of H₂O molecules and the metal-hydroxyl functional groups on the surface.¹² Song *et al.* investigated the mechanism of the COS hydrolysis reaction over a MgAlCeO_x hydrothermalite-like catalyst.¹³

^aDepartment of Mechanical Engineering, Wuhan Vocational College of Software and Engineering, Wuhan 430205, China

^bFaculty of Environmental Science and Engineering, Kunming University of Science and Technology, Kunming 650500, China. E-mail: save24176@126.com; Fax: +86-0871-65926040; Tel: +86-0871-65926040

^cPingxiang Huaxing Environmental Protection Engineering Technology Co., Ltd, Pingxiang, 337022, China

† Electronic supplementary information (ESI) available. See DOI: <https://doi.org/10.1039/d4ra03801k>



The presence of hydroxyl M–OH on the catalyst surface enhanced the hydrolysis process while providing more sites for organic sulfur adsorption. Therefore, hydroxylation modification on the ZrO₂ surface can be employed to enhance the hydrolysis process of organic sulfur. However, studies on the catalytic hydrolysis of CH₃SH and C₂H₆S using hydroxylated ZrO₂ are lacking, and the reaction mechanism has not been clarified. Therefore, it is necessary to propose a catalytic hydrolysis reaction mechanism of CH₃SH and C₂H₆S on hydroxyl ZrO₂ through theoretical studies.

This work presents a systematic investigation of the competitive adsorption process of CH₃SH and C₂H₆S, the catalytic hydrolysis reaction mechanism, and the catalytic role of surface hydroxyls. The investigation is conducted using a density-functional theory (DFT) approach. Additionally, the effects of ZrO₂ and surface hydroxyl groups on the hydrolysis reaction pathway are presented.

2. Computational method

ZrO₂ has been identified as a suitable catalyst for hydrolysis reactions in experimental and theoretical studies.¹⁴ Additionally, the ZrO₂(100) surface exhibits suitability for surface hydroxylation modification.¹⁵ Therefore, in this study, cubic ZrO₂ was employed to construct hydroxyl-modified ZrO₂. The geometries and energies for the catalyst (hydroxyl-modified ZrO₂), reactants (CH₃SH, C₂H₆S, H₂O), intermediates (IM), products, and transition states (TS) were calculated using Material Studio 2017 with the Dmol³ module.^{16,17} The GGA/PBE method employed herein provides a precise description of the interactions between electrons and encompasses a diverse range of material systems, thereby making it a highly prevalent choice in studies involving metal-containing catalytic systems.¹⁸ The calculation work employed the GGA/PBE method with a DNP 4.4 basis and spin-polarized set.¹⁹ The spin was set to unrestricted and the total charge was set to 0. In order to calibrate the energy, the basis set superposition error (BSSE) was taken into account in the calculation. To accurately describe weak interactions, dispersion-corrected density functional theory (DFT-D3 correction) was introduced.^{20,21} The SCF, energy, gradient, and displacement convergence tolerances were set to 1.0 × 10⁻⁶ Hartree (Ha), 1.0 × 10⁻⁵ Ha, 2.0 × 10⁻³ Ha Å⁻¹ and 5.0 × 10⁻³ Å, respectively. The cubic ZrO₂ was established according to the Crystallography Open Database. The space group of cubic ZrO₂ was FM-3M, and the lattice parameters are *a* = *b* = *c* = 5.070 Å. In this study, a five-layer ZrO₂ (100) surface with a p (3 × 3) supercell size was used. In order to construct the surface hydroxyl group, the ZrO₂(100) surface layer is composed of Zr atoms. The vacuum layer is 15 Å thick and all atoms are in a relaxed state. Additionally, hydroxyl groups were introduced and immobilised on the surface of Zr atoms to simulate hydroxylated ZrO₂ surfaces. Therefore, a surface hydroxyl structure of Zr–OH is constructed. The aforementioned parameters guarantee the accuracy of the resulting calculations.¹⁸ The transition states were searched, optimised and confirmed using the linear synchronous transit/quadratic synchronous transit/conjugate gradient (LST/QST/CG)

calculation method.²² The adsorption energies of the binary and ternary systems were calculated using eqn (1) and (2), respectively. *E*_A, *E*_B and *E*_C represented the energy of the catalysts and the gas molecules. *E*_{BSSSE} represented the energy of the basis set superposition error.

$$E_{\text{ads}} = E_{\text{AB}} - E_{\text{A}} - E_{\text{B}} + E_{\text{BSSE}} \quad (1)$$

$$E_{\text{ads}} = E_{\text{ABC}} - E_{\text{A}} - E_{\text{B}} - E_{\text{C}} + E_{\text{BSSE}} \quad (2)$$

3. Results and discussion

3.1 Adsorption of CH₃SH, C₂H₆S and H₂O over hydroxyl-modified ZrO₂

The adsorption properties of single and multimolecular gases on hydroxylated modified ZrO₂ surfaces were investigated. To elucidate the influence of hydroxyl groups on the adsorption process, two distinct adsorption sites were selected for the study: the Zr top site distant from Zr–OH (denoted as –(Zr)) and the hydroxyl site proximal to Zr–OH (denoted as –(OH)). The optimized adsorption configurations are depicted in Fig. 1, while the corresponding adsorption energies are presented in Table 1. The adsorption energies of the two gas molecules when simultaneously adsorbed at different sites were examined, and the corresponding adsorption configurations and adsorption energies are shown in Fig. S1 and Table S1,[†] respectively. Following structural optimization based on the calculated adsorption energies, it was determined that adsorption configurations (i), (iv), and (vii) represent the most stable configurations for different bimolecular systems. The current adsorption site was also identified as the global minimum energy point by the sorption module. Consequently, these three conformations were employed in Fig. 1 for comparison with the unimolecular adsorption conformations.

The adsorption energy results indicated that the adsorption of H₂O, CH₃SH, and C₂H₆S on the top site of Zr and the hydroxyl site was generated by chemisorption. The H₂O molecules exhibited a tendency to adsorb in close proximity to the Zr–OH,

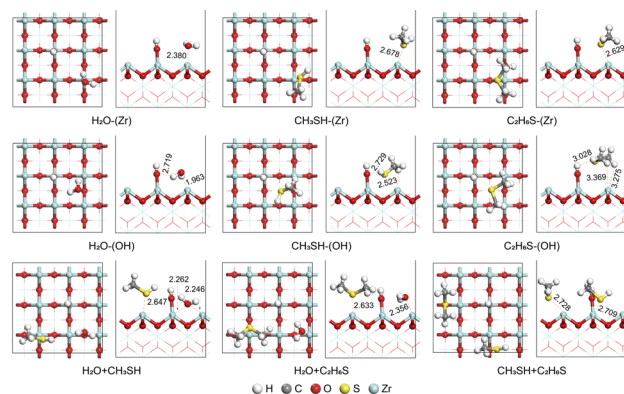


Fig. 1 Optimised adsorption configuration for CH₃SH, C₂H₆S and H₂O over hydroxyl-modified ZrO₂ (bond length in Å).

Table 1 Adsorption energy of CH₃SH, C₂H₆S and H₂O over hydroxyl-modified ZrO₂

Adsorptive geometries	Adsorption energy (kJ mol ⁻¹)
H ₂ O – (Zr)	-88.11
H ₂ O – (OH)	-123.51
CH ₃ SH – (Zr)	-192.68
CH ₃ SH – (OH)	-165.83
C ₂ H ₆ S – (Zr)	-164.89
C ₂ H ₆ S – (OH)	-114.63
H ₂ O + CH ₃ SH	-219.78
H ₂ O + C ₂ H ₆ S	-173.37
CH ₃ SH + C ₂ H ₆ S	-148.04

resulting in the formation of H–O and H–Zr bond interactions. The CH₃SH and C₂H₆S molecules exhibited a tendency to adsorb in close proximity to the Zr top site, resulting in the Zr–S bond interactions. This suggests that there is no competitive adsorption relationship between H₂O and CH₃SH/C₂H₆S, but that there is competitive adsorption between CH₃SH and C₂H₆S. The adsorption energies of the three gas molecules on the hydroxyl-modified ZrO₂ surface are in the order of CH₃SH-(Zr) > C₂H₆S-(Zr) > H₂O-(OH). This indicates that CH₃SH can preferentially adsorb on the Zr top site. When CH₃SH, C₂H₆S and H₂O are adsorbed simultaneously on the hydroxyl-modified ZrO₂ surface, the adsorption energies are in the order of H₂O + CH₃SH > H₂O + C₂H₆S > CH₃SH + C₂H₆S. This indicated that H₂O molecules are more capable of forming a two-gas molecularly stabilized adsorption structure with organosulfur molecules. The adsorption effects were attributed to the interaction between Zr and S/O atoms. Moreover, the adsorption energies of H₂O and CH₃SH/C₂H₆S are both greater than that of a single gas molecule when they are co-adsorbed on the hydroxyl-modified ZrO₂ surface. The results indicated that the presence of the H₂O molecule enhances and promotes the adsorption of CH₃SH/C₂H₆S. Conversely, the adsorption energies are lower than those of a single gas when co-adsorption of CH₃SH and C₂H₆S occurs. This is due to the fact that the adsorption of both CH₃SH and C₂H₆S on the ZrO₂ surface is caused by Zr–S interactions, resulting in competitive adsorption at the Zr top site. This results in a reduction in the stability of the adsorption process upon co-adsorption. This further substantiates the competitive adsorption relationship previously discussed. Consequently, the co-adsorption of H₂O and CH₃SH was observed to occur most stably on the catalyst surface.

3.2 Catalysis hydrolysis routes of CH₃SH over hydroxyl-modified ZrO₂

In order to investigate the catalytic hydrolysis of CH₃SH by hydroxyl groups and ZrO₂, the natural and catalytic hydrolysis routes of CH₃SH were investigated. The specific reaction routes are shown in Fig. 2. Route I and Route II are natural hydrolysis reaction processes. Route III is a hydrolysis reaction process involving hydroxyl groups, and Route IV is a hydrolysis reaction process involving only ZrO₂. The atomic migration process in Route IV was maintained consistent with Route II, which was

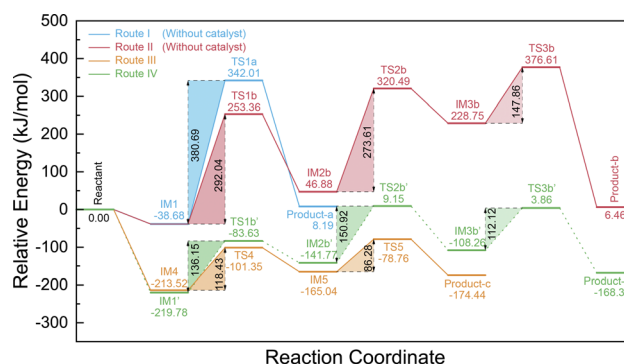


Fig. 2 Reaction routes and reaction energies for CH₃SH hydrolysis.

employed to assess the catalytic impact of ZrO₂. During natural hydrolysis, the intermediate (IM) and transition state (TS) structures in Route I and Route II were optimized and presented in Fig. 3. During catalytic hydrolysis, the optimized intermediates and transition states of Route III are shown in Fig. 4.

In Route I, CH₃SH and H₂O first undergo physical adsorption to form IM1, releasing 38.68 kJ mol⁻¹ of energy. After the breaking of the C–S bond in CH₃SH and the O–H bond in H₂O, TS1a is formed. This process requires overcoming a significant reaction energy barrier (380.69 kJ mol⁻¹). The combination of the hydroxyl group and CH₃ in TS1a, and the combination of the H atom and HS, results in the generation of Product-a (CH₃OH and H₂S). The relative energy of Product-a is 8.19 kJ mol⁻¹, which suggests that Route I is a heat-absorbing process. Therefore, Route I cannot occur spontaneously.

In Route II, C–S and O–H bonds are initially broken, with H atoms from the dissociation of the H₂O molecule migrating to CH₃ and the hydroxyl group migrating to HS, forming TS1b. This step requires the consumption of 292.04 kJ mol⁻¹ of energy

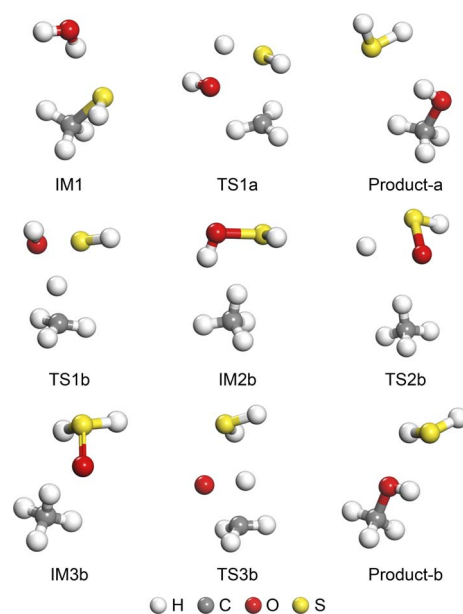


Fig. 3 IM and TS for CH₃SH hydrolysis (Route I and Route II).

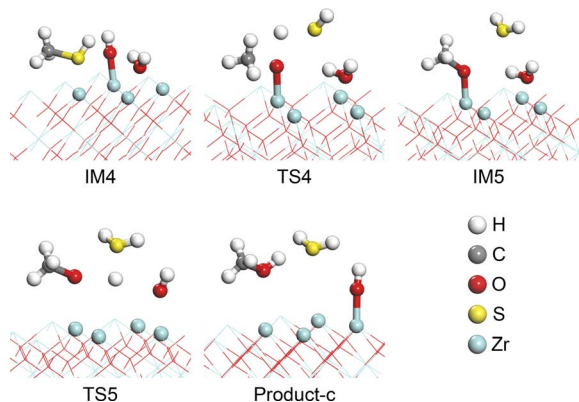


Fig. 4 IM and TS for CH_3SH hydrolysis over hydroxyl-modified ZrO_2 (Route III).

to be realised. With the combination of C–H and O–S bonds, IM2b was generated. Subsequently, the H atom on the O–H bond in IM2b undergoes an H-transfer. This results in the detachment of the H atom from the O atom and its migration to the S atom, forming H_2SO and generation of IM3b. This process necessitates the overcoming of a reaction energy barrier of $273.61 \text{ kJ mol}^{-1}$ (from TS2b). Subsequently, the S=O bond in HSHO is broken, and the O atom migrates to the vicinity of CH_4 , resulting in the breakage of the C–H bond and the production of TS3b. Furthermore, the O atom combines with the H atom and CH_3 to form CH_3OH . The process of IM3b to Product-b requires the consumption of $147.86 \text{ kJ mol}^{-1}$ of energy. The reaction energy barriers of the steps in Route II indicate that the reaction rate of Route II is affected by TS1b. Therefore, the production of HSOH is the rate-determining step of Route II. Compared to Route I, Route II has a lower maximum reaction energy barrier, which suggests that Route II is more likely to occur.

In Route III, CH_3SH and H_2O first adsorb around the hydroxyl group to form the stable adsorption structure IM4, which is realized by chemisorption. Next, the C–S bond in CH_3SH and the O–H bond in Zr–OH are broken to form TS4, which consumes $118.43 \text{ kJ mol}^{-1}$ energy. With the formation of S–H and C–O bonds, IM5 is produced. In this step, the H_2O molecule remains intact, and only CH_3SH is converted to H_2S through the surface hydroxyl groups. Then, the H_2O molecule is dissociated into H atoms and hydroxyl groups, while the Zr–O bond is broken. Product-c (CH_3OH and H_2S) is generated as the hydroxyl group binds to the Zr atom and the H atom migrates to CH_3O . This step necessitates overcoming the $86.28 \text{ kJ mol}^{-1}$ reaction energy barrier for the generation of TS5. The maximum reaction energy barrier in Route III is the process of TS4 production, which suggests that CH_3O formation is the rate-determining step. In comparison to Route II, the hydroxyl group significantly reduces the maximum reaction energy barrier during hydrolysis. Furthermore, the hydroxyl groups on the surface are capable of facilitating H-transfer, which is essential for the generation of H_2S , as well as the provision of free O atoms for the formation of C–O bonds. The depletion of surface hydroxyl groups can be replenished by the dissociation

of H_2O molecules, which effectively enhances the role of H_2O molecules in the hydrolysis reaction.

The reaction processes of Route IV and Route II are analogous. The change in reaction energy barriers indicates that ZrO_2 facilitates the hydrolysis process. In contrast to Route II, the participation of ZrO_2 in the hydrolysis reaction significantly reduces the reaction energy barrier of the HSOH generation step, resulting in the rate-determining step changing to HSHO generation. A comparison of Route III and Route IV revealed that ZrO_2 and hydroxyl exhibited disparate catalytic effects. The introduction of hydroxyl was found to be capable of further reducing the maximum reaction energy barrier.

3.3 Catalysis hydrolysis routes of $\text{C}_2\text{H}_6\text{S}$ over hydroxyl-modified ZrO_2

The natural and catalytic hydrolysis routes of $\text{C}_2\text{H}_6\text{S}$ were investigated to ascertain the catalytic effect of hydroxyl groups and ZrO_2 . The four reaction routes are depicted in Fig. 5. Route V and Route VI represent natural hydrolysis reaction processes. Route VII is a hydrolysis reaction process involving hydroxyl groups, and Route VIII is a hydrolysis reaction process involving only ZrO_2 . The atomic migration process in Route VIII was maintained consistent with that in Route VI, which was employed to assess the catalytic impact of ZrO_2 . The optimized intermediate (IM) and transition state (TS) structures in Route V and Route VI are illustrated in Fig. 6, and the optimized intermediates and transition states of Route VII are depicted in Fig. 7.

In Route V, $\text{C}_2\text{H}_6\text{S}$ and H_2O first undergo physical adsorption to form IM6, releasing $25.46 \text{ kJ mol}^{-1}$ of energy. This adsorption is weaker than that between H_2O and CH_3SH . After the breaking of the C–S bond in $\text{C}_2\text{H}_6\text{S}$ and the O–H bond in H_2O , TS6a is formed. This process necessitates the overcoming of a reaction energy barrier of $66.77 \text{ kJ mol}^{-1}$. The combination of the hydroxyl group and CH_3 in TS6a, along with the combination of the H atom and CH_3S , results in the generation of Product-a (CH_3OH and CH_3SH). The relative energy of Product-a is $26.68 \text{ kJ mol}^{-1}$, which indicates that Route V is a heat-absorbing process. Consequently, it can be concluded that Route V is not a spontaneous process. Subsequent to this, CH_3SH can undergo further hydrolysis reactions *via* Route II.

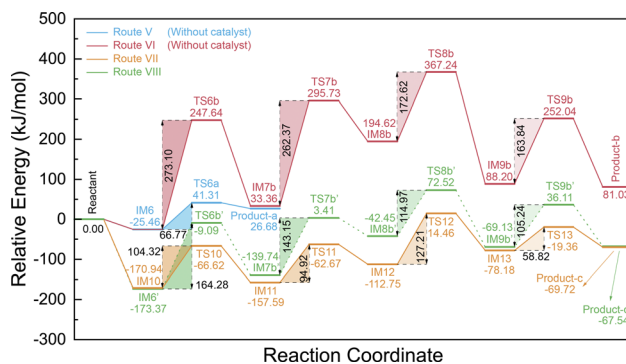


Fig. 5 Reaction routes and reaction energies for $\text{C}_2\text{H}_6\text{S}$ hydrolysis.

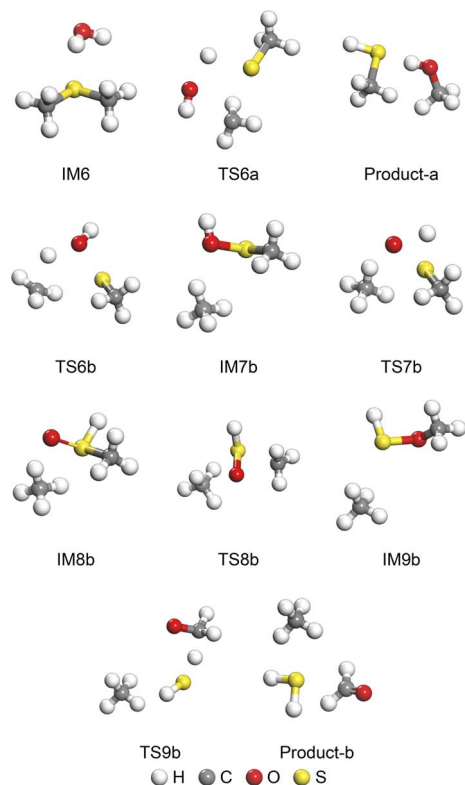


Fig. 6 IM and TS for C_2H_6S hydrolysis (Route V and Route VI).

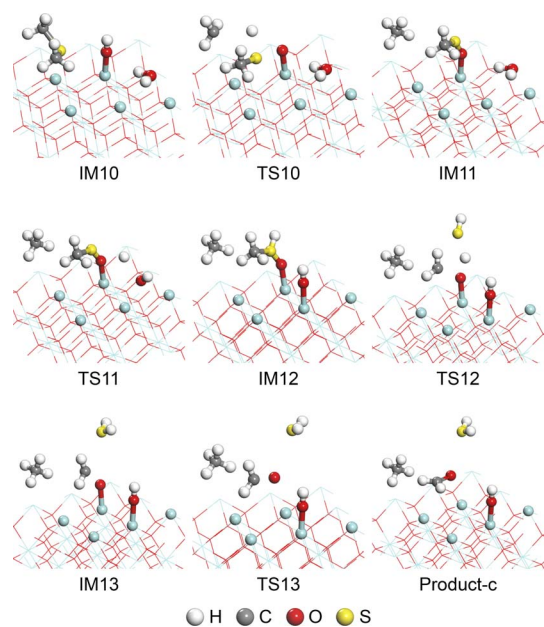


Fig. 7 IM and TS for C_2H_6S hydrolysis over hydroxyl-modified ZrO_2 (Route VII).

In Route VI, the C–S and O–H bonds are initially broken, with the H atoms from the dissociation of the H_2O molecule migrating to CH_3 and the hydroxyl group migrating to CH_3S , forming TS6b. This step requires the consumption of

$273.10 \text{ kJ mol}^{-1}$ of energy to be realised. The combination of the C–H and O–S bonds resulted in the generation of IM7b (CH_4 and CH_3SOH). Subsequently, CH_3SOH in IM7b underwent a H-transfer. The H atom on the O–H bond detached from the O atom and migrated to the S atom to form CH_3SHO , leading to the generation of IM8b. This process necessitates the overcoming of a reaction energy barrier of $262.37 \text{ kJ mol}^{-1}$ (from TS7b). Consequently, the C–S bond in CH_3SHO is broken, and the C–O bond is generated, thus forming CH_3OSH . The process of IM8b to IM9b requires the consumption of $172.62 \text{ kJ mol}^{-1}$ of energy. Subsequently, TS9b is generated as the C–H and S–O bonds in CH_3OSH are broken. The hydrolysis reaction is completed when the H atom completes its migration from the C–H bond to the S–H bond, and the final hydrolysis products are CH_4 , H_2S , and $HCHO$. The reaction energy barriers of the steps in Route VI indicate that the reaction rate of Route VI is affected by TS6b. Therefore, the production of CH_3SOH is the rate-determining step of Route VI. Compared to Route V + II, Route VI has a lower maximum reaction energy barrier, which suggests that Route VI is more likely to occur.

In Route VII, C_2H_6S and H_2O initially adsorb around the hydroxyl group to form the stable adsorption structure IM10, which is achieved through chemisorption. Subsequently, the C–S bond in C_2H_6S and the O–H bond in $Zr-OH$ are broken to form TS10, resulting in the consumption of $104.32 \text{ kJ mol}^{-1}$ energy. The formation of the C–H and S–O bonds results in the production of IM11. In this step, the H_2O molecule remains intact, with only C_2H_6S undergoing conversion to CH_3SO through the surface hydroxyl groups. Subsequently, the H_2O molecule is dissociated into H atoms and hydroxyl groups, while S–H is formed. The generation of IM12 occurs through TS11, with a reaction energy barrier of $94.92 \text{ kJ mol}^{-1}$. The breaking of C–S and C–H bonds in CH_3SO , which is accompanied by the migration of H atoms, results in the generation of IM13. This process requires overcoming a $127.21 \text{ kJ mol}^{-1}$ reaction energy barrier. The hydrolysis reaction is completed when the O atom completes its migration from the $Zr-O$ bond to the $C=O$ bond, and the final hydrolysis products are CH_4 , H_2S , and $HCHO$. The maximum reaction energy barrier in Route VII is the process of TS12 production, which suggests that the fracture of CH_3SHO is the rate-determining step. Compared to Route VI, the hydroxyl group greatly reduces the maximum reaction energy barrier during hydrolysis. In addition, the hydroxyl groups on the surface are also able to provide an H-transfer for the generation of CH_4 as well as free O atoms for the formation of S–O bonds. The depletion of surface hydroxyl groups can be replenished by the dissociation of H_2O molecules, which effectively enhances the role of H_2O molecules in the hydrolysis reaction.

The reaction processes of Routes VIII and VI are analogous. According to the alteration of reaction energy barriers, ZrO_2 facilitates the entire hydrolysis process. Nevertheless, ZrO_2 did not alter the rate-determining step of the hydrolysis reaction of C_2H_6S . When comparing Routes VII and VIII, ZrO_2 and hydroxyl exhibited disparate different catalytic effects, and the introduction of hydroxyl was capable of further reducing the maximum reaction energy barrier.

The co-promotion of ZrO_2 and hydroxyl groups was found to reduce the maximum reaction energy barriers of CH_3SH by $173.61 \text{ kJ mol}^{-1}$ and $145.89 \text{ kJ mol}^{-1}$, respectively. Furthermore, hydroxyl-modified ZrO_2 was observed to facilitate the hydrolysis process of CH_3SH to a greater extent than that of $\text{C}_2\text{H}_6\text{S}$.

3.4 Catalysis reaction mechanism of CH_3SH and $\text{C}_2\text{H}_6\text{S}$ over hydroxyl-modified ZrO_2

Based on the aforementioned findings, hydroxyl-modified ZrO_2 has been demonstrated to enhance and modify the hydrolysis reaction process of CH_3SH and $\text{C}_2\text{H}_6\text{S}$. Consequently, a reaction mechanism for the hydrolysis of CH_3SH and $\text{C}_2\text{H}_6\text{S}$ on the hydroxyl-modified ZrO_2 surface has been proposed and depicted in Fig. 8.

As illustrated in Fig. 8, the hydroxyl group on the ZrO_2 surface facilitated the production of H_2S and the formation of C–O bonds by providing free H atoms and free O atoms. Furthermore, the surface-free O atoms can effectively immobilize the intermediates CH_3 and CH_3S . The hydroxyl groups consumed on the surface can be replenished by the dissociation of H_2O molecules, maintaining the continuity of the hydrolysis reaction involving the hydroxyl groups. The hydrolysis of CH_3SH on the surface of hydroxyl-modified ZrO_2 proceeds as follows: $\text{CH}_3\text{SH} (+\text{H}_2\text{O}) \rightarrow \text{CH}_3\text{O} (+\text{H}_2\text{S}) \rightarrow \text{CH}_3\text{OH} (+\text{H}_2\text{S})$. The hydrolysis process of $\text{C}_2\text{H}_6\text{S}$ on the hydroxyl-modified ZrO_2 surface proceeds as follows: $\text{C}_2\text{H}_6\text{S} (+\text{H}_2\text{O}) \rightarrow \text{CH}_3\text{SO} (+\text{H}_2\text{O} + \text{CH}_4) \rightarrow \text{CH}_3\text{SHO} (+\text{CH}_4) \rightarrow \text{H}_2\text{S} + \text{CH}_2 (+\text{CH}_4) \rightarrow \text{HCHO} (+\text{CH}_4 + \text{H}_2\text{S})$.

4. Conclusions

This work investigates the competitive adsorption process of CH_3SH , $\text{C}_2\text{H}_6\text{S}$, and H_2O on the surface of hydroxyl-modified ZrO_2 using a density functional theory approach. Additionally, a detailed catalytic hydrolysis reaction mechanism is proposed. The adsorption process of CH_3SH , $\text{C}_2\text{H}_6\text{S}$, and H_2O on the surface of hydroxyl-modified ZrO_2 is attributed to chemisorption, with the Zr–S, H–O and H–Zr bonds playing a role. There is no competitive adsorption relationship between H_2O and

$\text{CH}_3\text{SH}/\text{C}_2\text{H}_6\text{S}$, but there is competitive adsorption between CH_3SH and $\text{C}_2\text{H}_6\text{S}$. It reveals the water-resistant properties of hydroxyl-modified ZrO_2 in desulfurization. The adsorption of CH_3SH on the Zr top site is favored over that of $\text{C}_2\text{H}_6\text{S}$. The hydrolysis of CH_3SH and $\text{C}_2\text{H}_6\text{S}$ is a heat-absorbing process that cannot occur spontaneously. The formation of CH_3O and the fracture of CH_3SHO are the rate-determining steps for CH_3SH and $\text{C}_2\text{H}_6\text{S}$ catalytic hydrolysis, respectively. The hydroxyl groups consumed on the surface can be replenished by the dissociation of H_2O molecules. The hydroxyl group on the ZrO_2 surface facilitated the production of H_2S and the formation of C–O bonds by providing free H atoms and free O atoms, enhancing the hydrolysis of CH_3SH and $\text{C}_2\text{H}_6\text{S}$. It provides theoretical guidance for industrial applications and the design of hydroxyl-containing hydrolysis catalysts.

Data availability

The data supporting this article have been included as part of the ESI.†

Author contributions

Xin Song contributed to the study's conception and design. Calculation, data collection and analysis were performed by Xin Song and Guihua Zhang. Guihua Zhang wrote the main manuscript text. All authors read and approved the final manuscript.

Conflicts of interest

There are no conflicts to declare.

Acknowledgements

This work was supported by the National Natural Science Foundation of China (22006058).

Notes and references

- P. J. Liang, D. C. Cheng, H. Y. Xu, C. Y. Xu, G. W. Chu, H. K. Zou, B. C. Sun and J. F. Chen, *Sep. Purif. Technol.*, 2024, **346**, 127374.
- W. Jiang, Z. Li, X. Kang, L. Luo, Y. Zhou, Q. Liu, K. Liu, X. Ji and G. He, *Gas Sci. Eng.*, 2024, **123**, 205243.
- G. Zhang, Q. Zhu, W. Zhang, Y. Zheng, Y. Cao, S. Liang, Y. Xiao, F. Liu and L. Jiang, *Inorg. Chem.*, 2022, **61**, 6083.
- H. Zhang, X. Liu, H. Xiao, F. Shao, T. Yan, D. Cheng, L. Han and D. Zhang, *Chem. Eng. J.*, 2024, **485**, 150003.
- X. Cao, T. Ai, Z. Xu, J. Lu, D. Chen, D. He, J. Liu, R. Tian, Y. Zhao and Y. Luo, *Sep. Purif. Technol.*, 2023, **307**, 122742.
- Y. Zhang, K. Li, X. Sun, X. Song, F. Wang, C. Wang, P. Ning and H. He, *Appl. Surf. Sci.*, 2021, **567**, 150851.
- T. Zhong, S. Tang, W. Huang, W. Liu, H. Zhao, L. Hu, S. Tian and C. He, *Appl. Catal., B*, 2024, **343**, 123476.
- R. M. Mohamed and A. A. Ismail, *Ceram. Int.*, 2022, **48**, 12592.

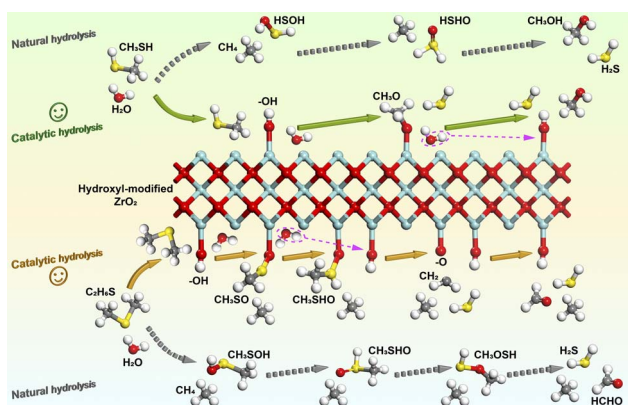


Fig. 8 Reaction mechanism of CH_3SH and $\text{C}_2\text{H}_6\text{S}$ hydrolysis over hydroxyl-modified ZrO_2 .

- 9 B. M. Alajmi, A. S. Basaleh, A. A. Ismail and R. M. Mohamed, *Surf. Interfaces*, 2023, **39**, 102899.
- 10 A. I. Ayesh and M. D. El-Muraikhi, *J. Mol. Model.*, 2022, **29**, 15.
- 11 N. Liu, P. Ning, X. Sun, C. Wang, X. Song, F. Wang and K. Li, *Sep. Purif. Technol.*, 2021, **259**, 118205.
- 12 X. Song, P. Ning, C. Wang, K. Li, L. Tang, X. Sun and H. Ruan, *Chem. Eng. J.*, 2017, **314**, 418.
- 13 X. Song, L. Sun, H. Guo, K. Li, X. Sun, C. Wang and P. Ning, *ACS Omega*, 2019, **4**, 7122.
- 14 X. Sun, W. Huang, H. Xu, Z. Qu, J. Wu and N. Yan, *Sep. Purif. Technol.*, 2023, **310**, 123194.
- 15 E. Osei-Agyemang, A. Dasan, R. Lucas, S. Foucaud, J. P. aul, S. Cristol and E. Laborde, *Appl. Surf. Sci.*, 2022, **576**, 151622.
- 16 B. Delley, *J. Chem. Phys.*, 2000, **113**, 7756.
- 17 L. Sun, P. Ning, X. Zhao, X. Song, K. Li, C. Wang, X. Sun and L. Jia, *Chem. Eng. J.*, 2021, **412**, 128752.
- 18 M. Ali, Z. Bibi, M. W. Younis and M. A. Iqbal, *Inorg. Chem. Commun.*, 2024, **160**, 111891.
- 19 J. P. Perdew, K. Burke and M. Ernzerhof, *Phys. Rev. Lett.*, 1996, **77**, 3865.
- 20 X. Song, X. Chen, L. Sun, K. Li, X. Sun, C. Wang and P. Ning, *Chem. Eng. J.*, 2020, **399**, 125764.
- 21 S. Wan, X. Song, X. Wang, C. Yuan, B. Wang, H. Chen, Y. Li, K. Ouyang and R. Chen, *Sep. Purif. Technol.*, 2022, **302**, 122158.
- 22 L. Jia, X. Song, L. Sun, S. Zhang, K. Li and P. Ning, *Chem. Eng. J.*, 2022, **429**, 132376.